NanoImpact 19 (2020) 100245

Contents lists available at ScienceDirect

NanoImpact

journal homepage: www.elsevier.com/locate/nanoimpact

Research paper

Influence of spray-coating process parameters on the release of TiO_2 particles for the production of antibacterial textile

Simona Ortelli[a,*], Franco Belosi[b], Rossella Bengalli[c], Fabrizio Ravegnani[b], Carlo Baldisserri[a], Massimo Perucca[d], Nuno Azoia[e], Magda Blosi[a], Paride Mantecca[c], Anna Luisa Costa[a]

[a] ISTEC-CNR, Institute of Science and Technology for Ceramics-National Research Council of Italy, Via Granarolo 64, 48018 Faenza, RA, Italy
[b] ISAC-CNR, Institute of Atmospheric Sciences and Climate-National Research Council of Italy, Via Gobetti, 101, 40129 Bologna, Italy
[c] POLARIS Research Centre, Dept. of Earth and Environmental Sciences, University of Milano – Bicocca, Piazza della Scienza 1, 20126 Milano, Italy
[d] Project HUB 360, C.so Laghi, 13, 10090 Buttigliera Alta, TO, Italy
[e] CeNTI, Centre for Nanotechnology and Smart Materials, Rua Fernando Mesquita, 2785, 4760-034 Vila Nova de Famalicão, Portugal

ARTICLE INFO

Editor: Bernd Nowack

Keywords:
TiO_2 nanoparticle
Spray-coating
Monitoring
Release
Exposure

ABSTRACT

Titanium dioxide (TiO_2) nanoparticles (NPs) are produced in high volume and widely used in manufacturing processes, raising potential occupational health concerns. Here, workers' exposure was assessed during production of antibacterial textiles, where TiO_2 NPs were impregnated onto 65% polyester 35% cotton textile surface by spray-coating. The influence of pressure, web speed and number of working spray nozzles to TiO_2 particles release was studied under different experimental conditions. Real-time monitoring was used to measure size-resolved particle concentration and lung-deposited surface area (LDSA) concentration using an optical particle counter and a diffusion charger, respectively, from both near- and far-field. Particles were sampled from the working area for off-line electron microscopy characterization, and suspensions of sampled particles were characterized by dynamic light scattering. Post-campaign data analysis was carried out and used for quantitative exposure safety assessment. Particle number concentration and LDSA results showed that pressure at the spraying nozzles (P) is the main parameter that influences the release of particles in the environment. Other process parameters studied (web speed and number of working spray nozzles) did not appear to significantly affect the release of particles. The particle number concentration in default experimental conditions (intermediate values for all process parameters; P = 2.3 bar, web speed = 6 m/min and number of working spray nozzles = 2) was quantified as $1.19\ 10^6$ # L^{-1}. Upon increasing the pressure, from 1.5 to 4.0 bar, near-field average mass and LDSA concentrations increased from 0.90 to 1.76 mg/m^3, and from 51.8 to 290.5 μm^2/cm^3, respectively. Average (avg) mass concentrations were well below the maximum recommended exposure limit of 2.4 mg/m^3 for fine TiO_2 particles proposed by the US National Institute for Occupational Safety and Health.

1. Introduction

In the last decade, nanotechnologies and engineered nanomaterials (NMs) have seen rapid development worldwide, with the consequent emerging problem of risks for workers (Kuhlbusch et al., 2018). Various strategies have been developed to assess the exposure to NMs in the workplace, integrating different aerosol measurement instruments and taking into account multiple parameters that may influence NMs toxicity (Asbach et al., 2017; Belut et al., 2019; Fonseca et al., 2015; Hussein et al., 2020; Koivisto et al., 2019, 2014; Nymark et al., 2020; Viana, 2016). Indeed, apart from the benefits associated with the growth of the nanotechnology industry, there are legitimate concerns about the potential consequences on human health (particularly for workers) and environment associated with exposure to NMs, in particular for ultrafine particles (UFP) having size smaller than about 0.1 μm (Gwinn and Vallyathan, 2006). Besides, UFP have a significantly greater inflammatory potential than fine particles (particle size above 100 nm) (Schmid and Stoeger, 2016). The increased surface area of UFP is apparently a most important determinant for their greater biological activity (Oberdürster, 2000). It has been reported that exposure to UFP particles worsens respiratory symptoms, leading to decreased lung function and asthma exacerbation (Donaldson et al., 2001; Ibald-Mulli et al., 2002; Pope III and Dockery, 2006).

The assessment of workplace exposure by inhalation of nano-objects and their aggregates and agglomerates is regulated by the EN 17058:2018 European Standard (EN 17058:2018), which provides

* Corresponding author.
E-mail address: simona.ortelli@istec.cnr.it (S. Ortelli).

https://doi.org/10.1016/j.impact.2020.100245
Received 18 May 2020; Received in revised form 23 July 2020; Accepted 3 August 2020
Available online 06 August 2020

guidance on the sampling and measurement strategies to be adopted and methods for data evaluation.

Human exposure to UFP occurs via the gastrointestinal tract, the skin, by injection during a medical treatment, and via the respiratory tract by inhalation. It is widely accepted that UFP intake in the respiratory tract is the most significant exposure route. In this work we address the potential health risk of workers operating in the nanomaterials industry, where manufactured products include the use of engineered UFP. The manufacturing context exposure scenario represents the most significant exposure route because exposure levels are expected to be at their highest (Nazarenko et al., 2014). Concerning the use phase of manufactured products, the inhalation exposure route has been identified as the likeliest one for those consumer products that are or can easily be dispersed as aerosol during their normal use, such as sprays or powders. On the other hand, inhalation is generally considered the primary exposure route because the matrix including UFP and NMs can be aerosolized into small droplets that can easily reach the lung tissue (Losert et al., 2014).

The health risk can be assessed based on UFP properties, such as size distribution, concentration, chemical composition, shape, and surface area/functionality (Ulrich et al., 2012). Due to both worker exposure potential and large-scale production volumes, spray-coating processes to produce antibacterial/self-cleaning surfaces by deposition of TiO_2 or Ag nanoparticles (NPs) are one of the most critical scenarios. Industrial spraying processes are among the primary causes of UFP dispersion into the air, especially at coating processes sites of (Viana, 2016). TiO_2 UFP, due to their properties, including photocatalytic and antimicrobial activities (Foster et al., 2011; Ortelli et al., 2014; Visai et al., 2011), are very promising coating materials for biomedical textiles (e.g. gowns, sheets, bandages, face masks) to prevent hospital infections. However, evidence has been put forward showing that exposure to TiO_2 UFP could adversely affect human health, especially via the inhalation route (Baranowska-Wójcik et al., 2020), and oxidative stress has been identified as the central mechanism involved in TiO_2-induced cytotoxic and genotoxic responses (Hanot-Roy et al., 2016; LeBlanc et al., 2010; Stoccoro et al., 2017). Furthermore, based on mechanistic studies and testing on animal models of exposure by inhalation, the International Agency for Research on Cancer (IARC) classified TiO_2 UFP as a potential carcinogenic factor from group 2B (probably carcinogenic to humans) (IARC, 2010). In addition, the US National Institute of Occupational Safety and Health (NIOSH) has determined that ultrafine TiO_2 is a potential occupational carcinogenic, but that there are insufficient data at this time to classify fine TiO_2 as an occupational carcinogenic. With the aim of ensuring safe and healthy working conditions, the NIOSH has provided a quantitative risk assessment using dose-response information from rat and human lung dosimetry modeling, and recommended exposure limits for fine and ultrafine (including engineered nanoscale) TiO_2 powders (Current intelligence bulletin 63, 2011).

Within the PROTECT (H2020-720851) European project, the present study proposes an approach for measuring and sampling TiO_2-based NMs in a well-defined (indoor) workplace in order to monitor the release of NMs during a spray-coating process, and suggest improved risk management strategies in occupational exposure scenarios. The proposed monitoring activity is part of a general methodology recommended by the Organization for Economic Cooperation and Development (OECD) (OECD, 2015). This consists of two fundamental steps: gathering information on the material, the process and any critical release points and basic exposure assessment, and endorsing measurement campaigns with instrumentation able to provide real-time data on the numerical concentration of UFP and other metrics of interest, as well as performing sampling for post-campaign off-line characterization (Boccuni et al., 2018; Koivisto et al., 2018). In this work, we conducted a measurements campaign in order to assess TiO_2 UFP exposure level during spray-coating deposition under different experimental conditions, studying the influence of three main process parameters (pressure, web speed and number of working spray nozzles) on real-time sampled data such as size distribution, concentration of particles released and lung-deposited surface area (LDSA), as well as off-line electron microscopy characterizations. Analysis of data obtained during monitoring measurements was carried out, and exposure control recommendations were given by comparing the mass concentration data with NIOSH recommended exposure limit.

2. Materials and methods

2.1. Materials and process description

Measurements were performed during the spray-coating process of aqueous suspensions of commercial Aeroxide® P25 TiO_2 nanoparticles from Evonik Degussa GmbH (Essen, Germany), characterized by a primary diameter about 20–30 nm. The spray atomization and deposition (SAD) line assembled at CeNTI (Centre for Nanotechnology and Smart Materials, Portugal) operates in continuous mode by means of a motor-powered roll-to-roll (R2R) mechanism comprising a transport conveyor and an electric oven. The conveyor design makes it possible to treat several types of foldable flat surfaces (like textiles and films). The specific experimental set up was employed to produce coated textiles with antibacterial properties. The size of the conveyor is about 7 m × 0.7 m. The deposition process works by means of an ultrasonic (US) multi-nozzle setup integrated in a serial scheme, driven at the frequency of 58 kHz. The distance between the multi-nozzle set-up and the substrate is manually adjustable; the optimal height was determined to be 40 cm, which produces a spraying cloud with a diameter of approximately 25 cm. For a proper operation of the nozzles, a compressed air line is available at the facility with manually adjustable pressure up to 4.0 bar. A local ventilation system located above the spray deposition system at a distance of 63 cm was found to be able to confine the release to the environment of drops and particles generated by the spray atomization process. The air exchange in the working environment was maintained by local exhaust ventilation (LEV) with 12 cm pipe internal diameter. The linear velocity of the air inside the tube is 1.8 m/s, accordingly LEV volume flow is estimated to be around 40 m^3/h. The work cycle consists of the following steps.

1. Loading the nanoparticles' suspension tank. Workers fill the tank connected with the nozzles, in this specific case with aqueous suspensions of P25 TiO_2 NPs.
2. Loading the fabric supply roll.
3. Unwinding the fabric from the supply roll.
4. Spray atomization deposition through the ultrasound-driven spraying nozzles, onto the moving fabric passing under the spraying stage.
5. Drying the sprayed fabric by passing it through the electric oven stage.
6. Rolling-up the functionalized textile.
7. Removing and storing the finished textile's roll.

The monitoring measurements were focused on step 4, identified as the hot spot of the exposure scenario (Simeone et al., 2019).

Six adjustable processing parameters were available:

1. pressure (from 1.5 to 4.0 bar)
2. web speed (from 2 to 10 m/min)
3. number of working spray nozzles (from 1 to 3)
4. nanoparticle suspension volumetric flow rate (fixed at 50 mL/min)
5. cone volume (which embeds two technical parameters: cone aperture and distance between the spraying nozzle and the surface being treated) (established at 6 L; d = 25 cm, h = 37 cm)
6. suspension concentration (kept constant at 4.50 g/L).

Another interesting parameter that could be studied is the nozzle type. Despite this, we decided not to change it as the spray-coating pilot

plant equipped by US nozzles is part of a European project (PROTECT, H2020-720851), changing the nozzle type falls outside the scope of our study.

Before running the probing campaign, we selected a sub-set of varying processing parameters and we devised a Design of Experiment (DoE) matrix in order to study the influence of these process parameters on the emission of particles. In order to minimize the number of experimental runs, we considered three levels for each identified relevant process parameter.

This parameter choice was motivated by two factors:

- the need of covering the wide range of technically feasible operating modes that are associated to different required functionalization levels.
- the need of monitoring parameters that were expected to have more influence on the nanoparticle dispersion into the environment.

The variation of pressure, web speed and number of working spray nozzles primarily influences the amount of deposited nanoparticle liquid suspension on the fabric, which is expected to determine different degrees of antibacterial performance; an increase in carrier gas pressure is expected to be associated with higher diffusion of droplets and greater droplets size onto the fabric; web speed is connected to production throughput, and the number of nozzles is associated to the size of the web to be treated in order to satisfy the requirement of surface treatment uniformity. On the other hand, nozzles' driving pressure increase involves a higher flow rate of gaseous carrier and a potentially larger diffusion of NPs into the environment. Web speed increase is associated with increased air turbulence at the fabric boundary layer, which in turn may increase remixing and diffusion of NPs-carrying aerosols into the environment. Variation of spray nozzles number determines a change in the nanoparticle source intensity, likely resulting in a different rate of delivery of NPs into the environment.

In accordance to the described principles, the experimental plan considered varying pressure, web speed and number of working spray nozzles during the monitoring activities, also defining the minimum, medium and maximum value for each parameter, as reported in Table S1.

We selected three levels for each parameter in compliance with the values that are technically applicable to the processing unit and significant in determining the different operating regimes. The experimental full factorial matrix is given in Table S2, Supporting information. This allowed monitoring the spray coating process in different experimental conditions corresponding to the different operating modes. In contrast, the following processing parameters were kept constant:

- nanoparticle suspension volumetric flow rate (50 mL/min)
- cone volume (6 L; d = 25 cm; h = 37 cm)
- suspension concentration (4.5 g/L)

This choice was determined either because variation of some of these parameters is not performed in practice, or because the variation of the parameter would only provide a redundant set of processing parameters determining the same operating mode, which can be obtained by varying only the first three selected parameters.

We assessed the environmental and processing features reported in Fig. 1, obtaining the following values:

- spray coating facility floor area ~42 m^2
- spray coating facility volume ~126 m^3
- spray coating processes run indoor at atmospheric pressure and ~20 °C temperature;
- personnel operating the spray coating plant consisting of a single worker equipped with personal protective devices (gloves, lab coat, glasses, mask).

In order to assess the influence of the selected varying processing parameters on nanoparticles diffusion in the environment, we performed the monitoring campaign during the spraying unit active run, according to the selected operating mode, processing protocol, and the characterized environmental features.

2.2. Methods

We measured particles number concentration, size distribution, and lung-deposited surface area (LDSA) simultaneously at two locations 1 m and about 4 m distant from the source, which will be referred to as near-field (NF) and far-field (FF), respectively. Fig. 1 shows a schematic of the layout. The monitoring campaign was conducted including both real time measurements and post-campaign off-line analysis of particulate matter collected on filters:

- Diffusion Size Classifiers: Partector (Naneos particle solutions, GMBH) and DiSCmini (Testo) which can determine by diffusion charging the Lung-Deposited Surface Area (LDSA, expressed in $\mu m^2/cm^3$) (Partector) and the particle number concentration and LDSA (DiSCmini), at 1 s acquisition time. Particle size range for Partector and DiSCmini is 10 ÷ 10,000 and 10 ÷ 300 nm, respectively. Both monitors are based on unipolar diffusion charging of the particles to determine the alveolar lung deposited surface area (LDSA) concentration. The DiSCmini additionally provides estimates of mean particle size and particle number concentration (Todea et al., 2017).
- Optical Particle Counter (OPC, Grimm mod. 11-A) measures the size-resolved particle number concentration in the size range 0.25 ÷ 20 μm. Particle number concentration (#/L) data are collected at 6 s acquisition time.
- Climatic probe (PCE-THB 40) for real-time measurement of climatic parameters, such as temperature (RT, °C) and relative humidity (RH, %).

We carried out airborne particle sampling on polycarbonate (PC) filters (Whatman Nuclepore porosity 100 nm) under 4 L/min forced flow conditions. A, sampler unit (Bulldog, XearPro, Italy) was used.

We used Field Emission Scanning Electron Microscopy (FESEM - Carl Zeiss Sigma NTS, Gmbh Öberkochen, Germany) coupled with an energy dispersive X-ray (EDX) micro-analyzer (EDS, mod. INCA Energy 300, Oxford instruments, UK) to analyze particles collected on the filters. We recorded FESEM images at different magnifications on coupons of PC filters attached onto an aluminum holder using carbon tape. Samples were gold-coated (thickness = 5 nm). FESEM/EDX analysis allowed assessing overall particles' distribution on the filter as well as particles' structural characterization.

We extracted particles collected on the filters in water in an ultrasonic bath for 20 min. The so-obtained suspensions were centrifuged at 5000 rpm and a spin time of 20 min using an Ultra-Centrifugal Filter (UCF) unit (Amicon Ultra-15, 3 kDa, Millipore), which allowed obtaining suspension samples at a high concentration of NPs. In order to determine particle size distribution by intensity we analyzed the concentrated suspensions by means of dynamic light scattering (DLS), performed with a Zetasizer nano ZSP (model ZEN5600, Malvern Instruments, UK). Each sample underwent three measurements, and we obtained size values by averaging these measurements.

Time-sheets of the full measurements in chronological order associated with each run, consisting of 2 min of spray coating and 10 min of break (the latter being the time requested to re-establish particles' concentration to near-background levels) are summarized in Table S3.

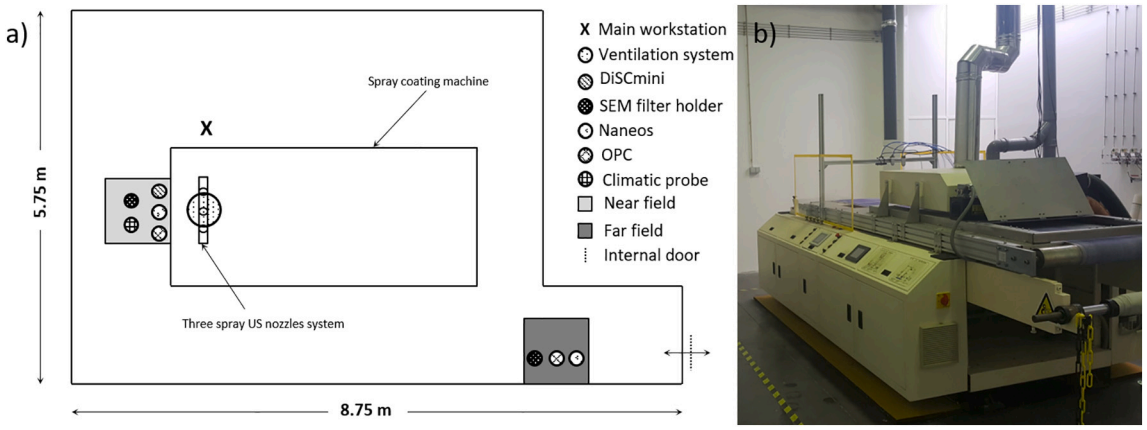

Fig. 1. Layout of the process area and instrumentation. a) Scheme of the process area (5.75 m × 8.75 m). The white box represents the spray-coating machine containing the three-US-nozzle spray system and the local ventilation system above them, which was on at all times. The X marks the main working station, where the operators load the nanosuspensions for the coating process. The light grey box, at 1 m from the loading station, represents the near field (NF) source, where the instruments (OPC, DiSCmini, Naneos, climatic probe) and the SEM filter holder were placed. The dark grey box, at 4 m from the working station, represent the far field (FF) source with the OPC and Naneos instruments and the SEM filter holder. b) Photo of the process area.

3. Results and discussion

3.1. Particles number concentrations, size distribution and lung deposition surface area

We analyzed particles number concentrations, size distribution, and lung deposition surface area (LDSA) data considering two main phases: pre-activity (background, BG) and spraying activity, comprising spray deposition through US spray nozzles (2 min) followed by a 10-min break. The spray deposition phase consists of 15 runs, which were designed by combining the different process parameters (Table S2).

Before starting the first spraying activity, while the spray coating machine was turned off, we determined the BG signal in both NF and FF. When the BG was first measured, the plant had been idle during about the previous ten days, so the initial background measurement was not influenced by the process. Therefore, any increase of particles concentration above BG due to spray activity can be attributed to the spray process. OPC data showed a low BG concentration of particles, average values in both NF and FF being 3.6 10^4 and 3.0 10^4 # L^{-1}, respectively. The size distribution showed the presence of relatively small particles; more specifically, we found 98% of BG particles to have a diameter smaller than 0.5 μm, as shown in Fig. S1.

In order to study the influence of process parameters on the release of particles, in terms of concentrations, size distribution and LDSA, we combined the data obtained in NF from runs in different experimental conditions. We focus our attention on data obtained in NF, as these are more influenced by experimental conditions.

By investigating the dependence on web speed and number of active nozzles at constant 1.5 bar nozzle pressure (Fig. 2a), we found that - during single-nozzle spraying - the particles concentration, measured by OPC increased as web speed was increased from 2 to 10 m/min, thus supporting the hypothesis that air entrainment and turbulence level increase due to shear effects of the fabric in air, facilitating dispersion of the nanoparticles into the environment. Conversely, we found lower UFP concentrations when the number of working spray nozzles was increased to three, likely due to coalescence phenomena induced by multi-nozzle spraying (Nijdam et al., 2004; Santolaya et al., 2013). Upon increasing spraying nozzle pressure to 2.3 bar (Fig. 2b), an unclear dependence of particles concentration on web velocity during two-nozzle spraying was observed (values and error bars are compatible with no dependence at all on web velocity). Moreover, spray nozzle pressure to 2.3 bar (Fig. 2b) did not significantly change particles' concentration, as they ranged between 1.1 10^6 # L^{-1} to 1.4 10^6 # L^{-1}. We found again a marginally smaller particle concentration at 6 m/min web speed during three-nozzle spraying (1.1 10^6 # L^{-1}) as compared to 1-nozzle spraying (1.2 10^6 # L^{-1}). Finally, at the maximum pressure studied (P = 4.0 bar; Fig. 2c) we found no dependence of concentration on web velocity, both with one and three active nozzles. Unlike what was previously observed (Fig. 2a), data as a whole stand against any coalescence effect at P = 4 bar.

We then investigated the correlation between particles concentration and nozzle pressure. As shown in Fig. S2, the main parameter affecting the concentration of airborne particles is the pressure at the nozzles, irrespective of the number of active nozzles during spray coating. No clear dependence on other process parameters (web speed and number of active nozzles) did emerge. The most important operative parameter affecting LDSA during plant operation is the pressure at the spraying nozzles: increasing nozzle pressure from 1.5 bar to 2.3 bar and to 4.0 bar causes the averaged LDSA value measured by Partector to increase from 51.8 $\mu m^2/cm^3$ to 137.8 $\mu m^2/cm^3$ and to 290.5 $\mu m^2/cm^3$, as shown by the NF data in Fig. 3. Good instrumental correlation between LDSA values from DiSCmini and Naneos gauges is demonstrated by the slope of linear regression and linear correlation coefficient equal to 1.07 and 0.98, respectively. LDSA was chosen as a convenient metric for aerosol concentration, due to LDSA having been shown to correlate well with toxic effects (Duffin et al., 2002; Fissan et al., 2007; Oberdörster et al., 2004; Oberdürster, 2000). Few literature data are available on LDSA from exposure to UFP. A recent study (Geiss et al., 2016) compared the levels of LDSA in selected occupational and non-occupational environments; data showed that high peak values of LDSA and particles concentration were measured during activities in a canteen kitchen (max LDSA 3927 $\mu m^2/cm^3$, average 415 $\mu m^2/cm^3$) and in a chamber test during tobacco cigarette burning (LDSA peak 784 $\mu m^2/cm^3$). Data about LDSA were related to occupational activities in which engineered UFP are scanty, and often LDSA occupational measurements were limited to welding activities, were values could reach an average LDSA value of 137 $\mu m^2/cm^3$. In different urban areas, average LDSA values are usually below 100 $\mu m^2/cm^3$ (Hama et al., 2017), evidencing the important contribution of indoor activities as sources of UFP exposure. In our experimental conditions, at a pressure of 4 bars in NF, the LDSA reaches values of 200–400 $\mu m^2/cm^3$, comparable with those detected during cooking activities in an occupational environment, while at lower pressures (1.5 and 2.3 bars) LDSA values do not exceed 150 $\mu m^2/cm^3$. Finally, as expected, in the proximity of the spray atomization unit identified as the hot spot of the exposure scenario, a greater particles' concentration, expressed as both particle number (#/L) and LDSA ($\mu m^2/cm^3$) (Fig. S3) was observed. In fact, comparing NF and FF data collected with both Naneos and OPC

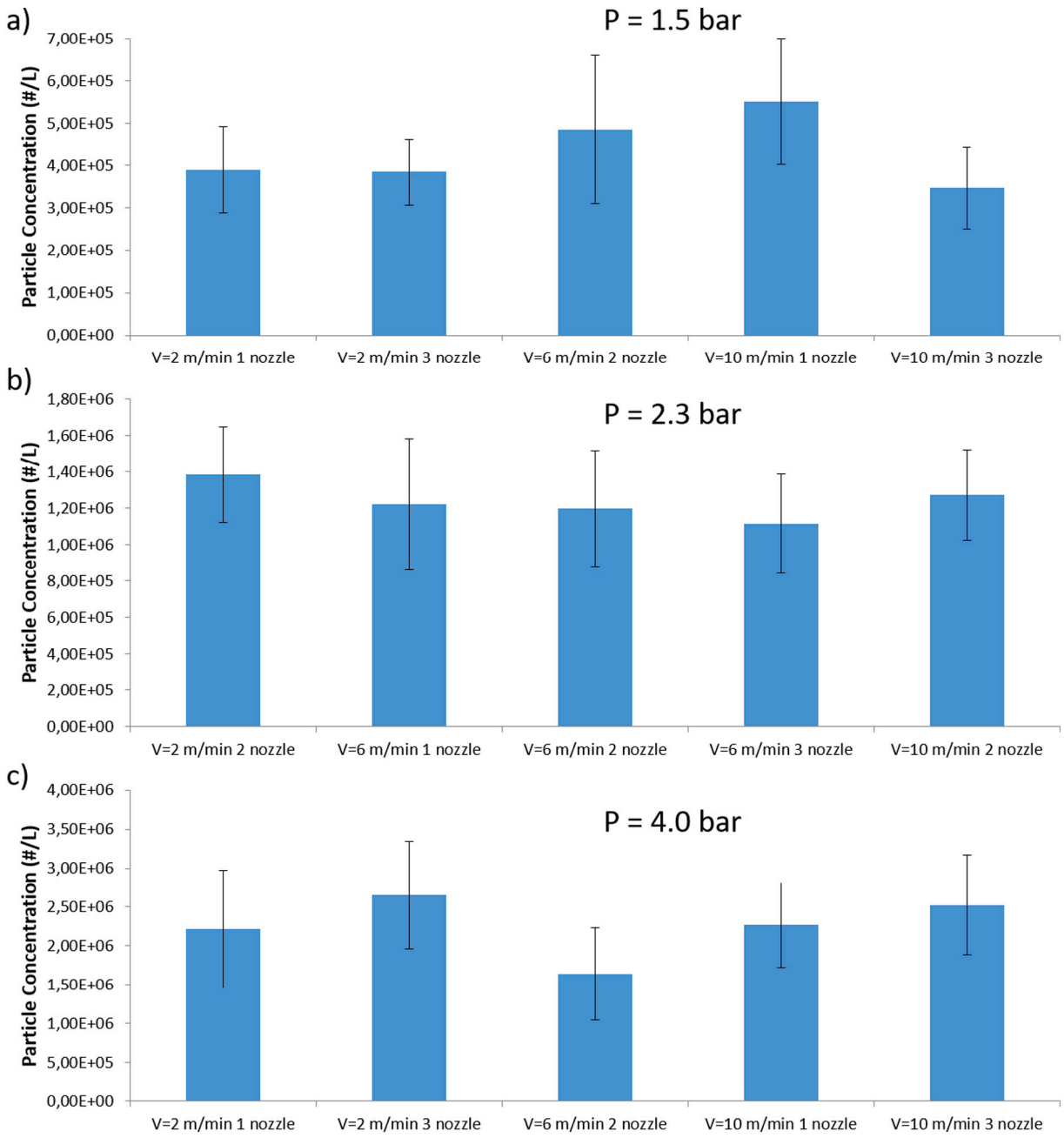

Fig. 2. Particle number concentration under different experimental condition as to speed and number of active spray nozzles at: a) P = 1.5 bar (avg conc ≈ 4.3 10^5 # L^{-1}); b) P = 2.3 bar (avg conc ≈ 1.2 10^6 # L^{-1}), and c) P = 4.0 bar (avg conc ≈ 2.3 10^6 # L^{-1}). Note the different scales on the particle concentration axis. Data collected by OPC (0.25 ÷ 20 μm diameter range).

gauges, reported in Fig. S3a and b respectively, a greater impact at NF zone was observed in real time. The lower particle concentration found could be attributed to the ventilation system, located above the spray US nozzles unit as shown in Fig. 1. These data again confirmed good instrumental correlation between Naneos and OPC.

As regards particle size distribution (Fig. S4), considering OPC data over the 250 nm ≤ Dp ≤ 25 μm dimensional range, a general decreasing trend of the abundance of suspended particles vs. increasing particle size was observed, with particles in the 0.2 ÷ 1 μm range being more abundant. Moreover, we found that high web speed and multi-nozzle spraying tend to produce higher particle number concentrations. Data on UFP particles size distribution are not available at present due to instrumentation limitations. With data so far available (Fig. S4) it is difficult to speculate on the correlations between particle size distribution and the process parameters studied; however, in NF a significant correspondence between number of active nozzle and particle size was found. In fact, as shown by Fig. 4, the coarse to total particles ratio increases as the number of active spray nozzles increases, which might be due to a higher number of coalescence events from a larger overlap of the nozzle's spray plumes (Francia et al., 2016a, 2016b). From Fig. S5 it is clear in that - at all values of pressure investigated – with three active spray nozzles the concentration of coarse (> 1 μm) particles increased. Besides, it is clearly observed that at intermediate process conditions (6 m/min web speed and 2 working spray nozzles) finer particles number concentration tends to increase at higher nozzle pressure, whereas that of coarser particles decreases (Fig. S6). Fig. 5 shows the relative percent difference between particle number concentration at 2.3 bar and 4.0 bar with respect to 1.5 bar.

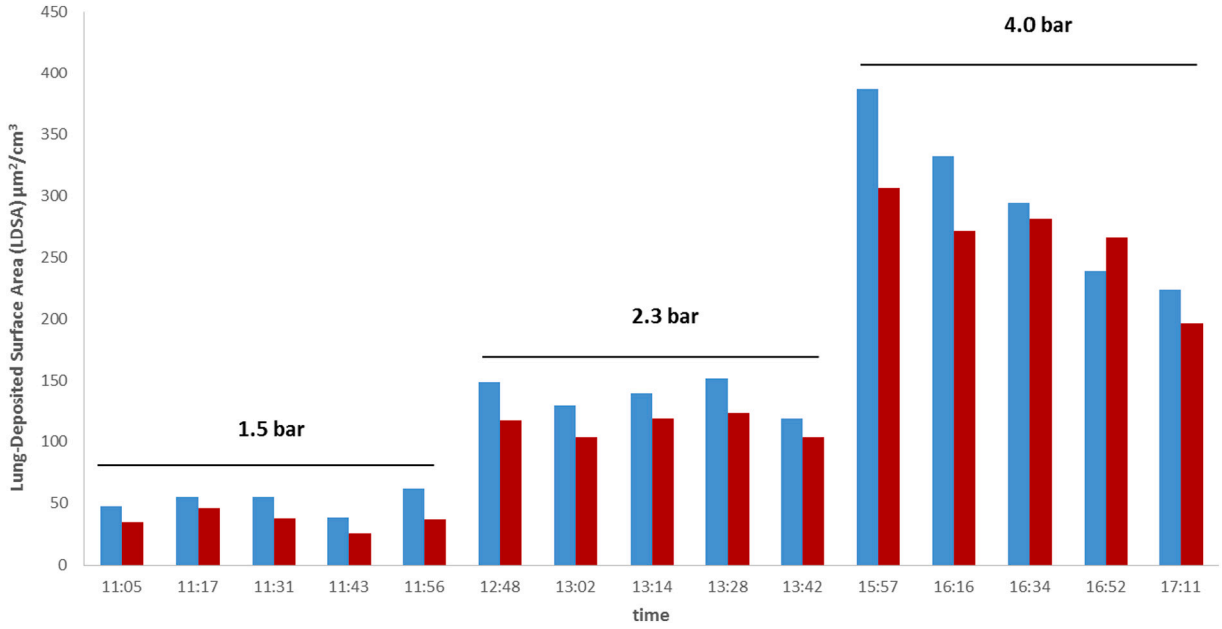

Fig. 3. Increase of lung-deposited surface area with increasing pressure at the nozzles. Data collected by Naneos (blue) and DiSCmini (red) in NF.

This trend was further confirmed by particle size distribution data obtained using DLS on suspensions of extracted particles, as reported in Table 1. Indeed, upon increasing the pressure from 1.5 to 4.0 bar, the average diameter of particles from both NF and FF filters decreases (from 507 to198 nm and from 1.4 µm to 375 nm, respectively), as found by D. Nuyttens and colleagues demonstrating that higher spray pressure corresponds to a smaller droplet size spectrum (Nuyttens et al., 2007).

3.2. FESEM analysis on filters

We performed FESEM analysis of filters obtained from ambient air sampling. Filters were obtained at each pressure value studied (1.5, 2.3 and 4.0 bar) during five iterations at the same pressure, both in NF and FF. FESEM analysis on a filter obtained at 1.5 bar nozzle pressure showed the presence of low amounts of released particles, both as single UFP and as UFP agglomerated or aggregated in micrometric granules (Fig. 6), which agrees with other studies on the release of aerosolized UFP during spray processes (Bekker et al., 2014; Hagendorfer et al., 2010; Park et al., 2017). The physical form of the product, primarily as to size and agglomeration state, is a key factor for the emission potential of NPs in the indoor environment. For powders, the emission potential is determined by the dustiness of the material handled, defined as the intrinsic potential of a determined NP to become airborne. It is known that size and agglomeration state influence the dustiness of powders, ultrafine powders displaying high dustiness, agglomerated powders displaying medium dustiness, and pellet-type solids featuring low dustiness, dustiness in turn being known to affect inhalation exposure(Viana, 2016). We found qualitatively that in FF the concentration of released particles is very low (Fig. 6a and b), whereas in NF it was found to be higher (Fig. 6c and d). Upon increasing the pressure of the spray process to 2.3 bar, a general increase of released particles was observed (Fig. 7), more accentuated in NF (Fig. 7c and d). At the highest value of pressure studied (P = 4.0 bar), the concentration of released particles is very high, both in NF and FF. In fact, differences between NF and FF that were observed in the previous cases are not visible (Fig. 8). At P = 4.0 bar we could observe both structural morphologies, i.e. single NPs and micrometric granules. In fact, at high magnifications (Fig. S7) it is possible to observe the nanometric size of released NPs (Fig. S7a and c), showing the typical diameter of P25 TiO_2 powder (about 20–30 nm according to supplier specification, confirmed by Jensen et al. (2006), as well as micrometric granules (Fig. S7b and d) that are formed during the SAD that leads to NPs agglomeration or aggregation (Francia et al., 2017). Moreover, EDX analysis confirmed that both single NPs (Fig. S8) and micrometric granules (Fig. S9) consist of TiO_2, as expected. Ti was detected along with C, O and Au (deposited during FESEM sample preparation). FESEM analyses on filters qualitatively confirms the data directly measured.

3.3. Mass concentration

A qualitative comparison with the recommended exposure limit (REL) was obtained by converting the particle number concentration into particle mass concentration. This conversion is always subjected to uncertainties due to unknown parameters needed to transform an optical particle diameter into an aerodynamic particle diameter. On the other hand, the averaged mass concentrations might be so low that results from gravimetric analysis are under the detection limit of the technique, especially in case of short sampling time.

Particle number concentration data (#/L) collected by OPC over the 0.25 ÷ 20 µm size range were converted to mass concentration assuming 4.2 g/cm^3 TiO_2 density, in order to compare such values with the recommended exposure limit (REL) for fine TiO_2 particles, quantified by the National Institute for Occupational Safety and Health (NIOSH) (Current intelligence bulletin 63, 2011) as 2.4 mg/m^3 (10-h time-weighted average (TWA) during a 40-h work week). NIOSH recommends airborne exposure limits of 2.4 mg/m^3 and 0.3 mg/m^3 for fine and ultrafine TiO_2. Considering the coalescence phenomena induced by the spraying process, agglomeration or aggregation of primary NPs (20–30 nm) does occur, with the consequent formation of larger particles (see DLS size mean diameter reported in Table 1). Based on this, it is supposed that the respirable fraction mainly consists of aerosolized micrometric particles. Nevertheless, in case of NF samples, collected at the highest pressures, we can hypothesize from both DLS and SEM analysis a significant contribute of ultrafine fraction with a corresponding DLS mean size around 200 nm. For this reason, data reported on Figs. S10, S11, S12, considered both fine and ultrafine RELs, being the last relevant for worst exposure scenario. From the analysis of mass concentration, calculated at different nozzle pressures in NF and FF conditions, we can conclude that in all cases, only the minimum concentrations detected stay below the UFP REL (0.3 mg/m^3). While if comparing values to REL of fine particles, data show that at the lowest pressure value (1.5 bar) only the maximum measured

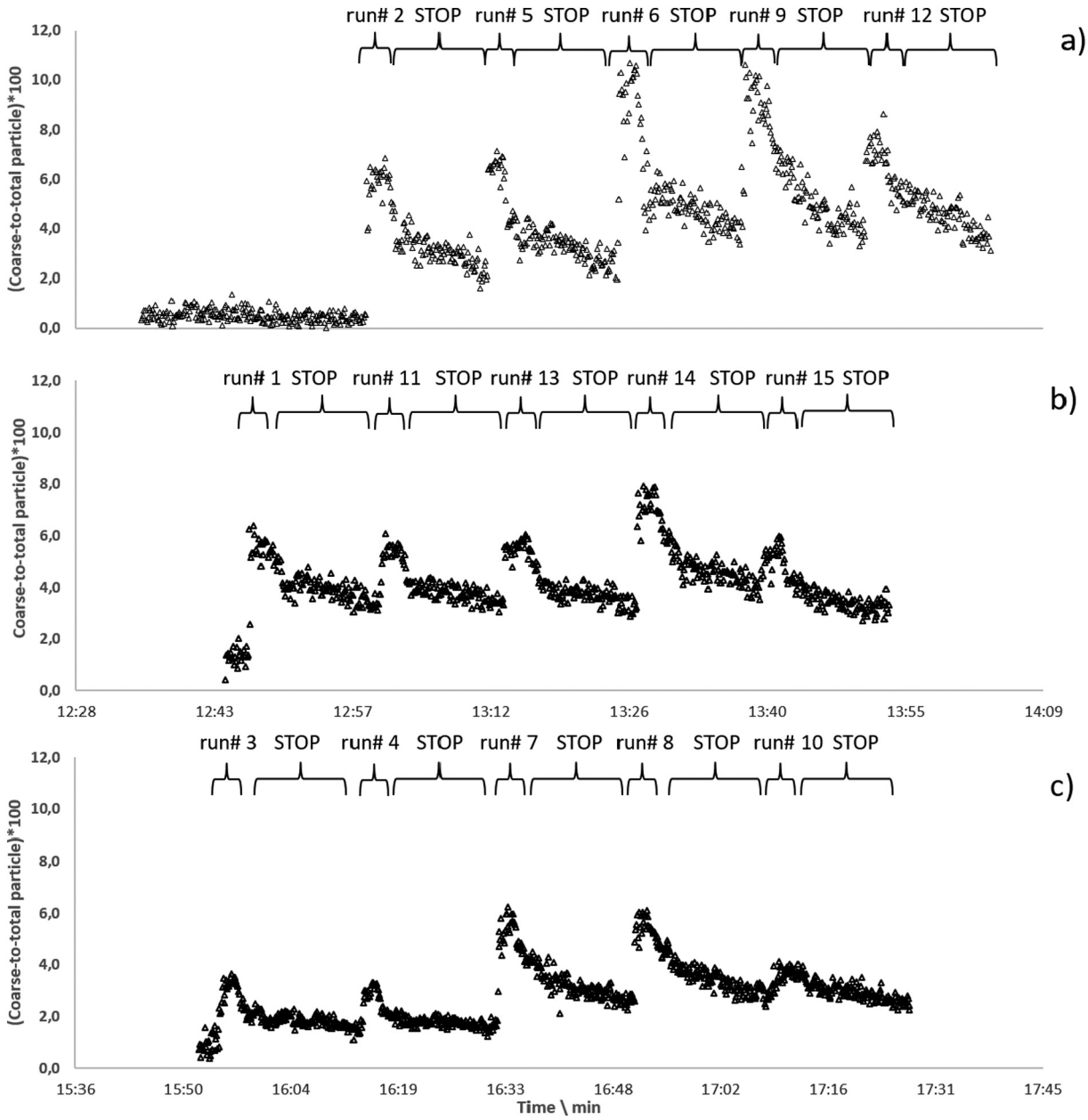

Fig. 4. Coarse (1 ÷ 20 μm diameter range) to total particles ratio during runs at pressure a) 1.5 bar with number of spray nozzles equal to: 1 (Run # 2 and 5); 3 (Run # 6 and 9); 2 (Run # 12); b) 2.3 bar with number of spray nozzles equal to 2 (Run # 1, 11 and 13), 3 (Run # 14) and 1 (Run # 15); c) 4.0 bar with number of spray nozzles equal to 1 (Run # 3 and 4); 3 (Run # 7 and 8); 2 (Run # 10). All process parameters characterizing each run are reported in Table S2. Data collected by OPC.

value (2.65 mg/m^3) was slightly higher than the REL, whereas the medium one measured in the FF was much lower (Fig. S10a). Similarly, in NF (Fig. S10b), we found that only the highest values, corresponding to peaks collected during the spray coating, were higher than REL.

Upon increasing the pressure at the nozzle to 2.3 bar (Fig. S11), a general increase of mass concentration is observed, in particular medium values are coming closer to the REL. However, in FF (Fig. S11a), only the maximum values corresponding to the spray activities exceed the REL, but in NF (Fig. S11b) mass concentration values are generally quite high. At the highest pressure value studied (P = 4.0 bar), mass concentration increases significantly (Fig. S12) both in the near and the far field. In fact, medium values, both in the near and far field (1.76 and 1.89 mg/m^3 respectively), are quite close to the REL, but they stay anyway below the REL. Besides, maximum FF values are much higher than the REL, exceeding the REL by 0.25, 2.64 and 6.1 mg/m^3 at P = 1.5, 2.3 and 4.0 bar, respectively. Even higher differences between maximum values and REL are found in NF, 3.8, 8.2, 10.5 mg/m^3 at P = 1.5, 2.3 and 4.0 bar, respectively. The maximum mass concentration was found at P = 4.0 in NF (12.9 mg/m^3), but this peak value was reached only two times during the spraying process at that pressure. However, even in the case of maximum concentration, we should consider that the REL is given as a time-weighted average (TWA) concentration for up to 10 h per day during a 40-hour work week, and this timing does not represent the real working condition for workers involved in the spray-coating process examined here. In fact, the pilot plant involved in this study is sufficiently automated requiring only initial settings and occasional checking by the workers. Thus it is reasonable to think that the workers are subjected to lower concentrations than those measured, as they have a workplace in the same room as the pilot plant only for short time.

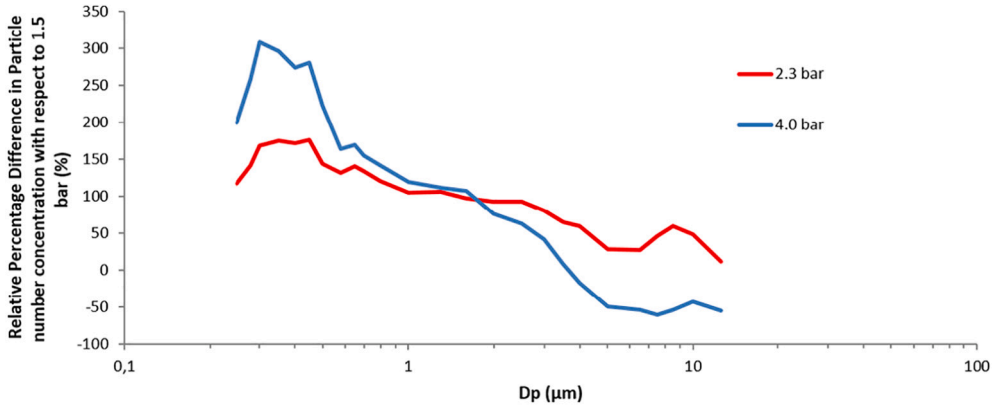

Fig. 5. Relative percent difference between particle number concentration at 2.3 bar and 4.0 bar with respect 1.5 bar. Intermediate web speed (6 min/m) and number of working spray nozzles (n = 2). Data collected by OPC.

Table 1
Average diameter (d_{DLS}, nm) and polydispersity index (PdI) of particles extracted from the filters collected at each pressure value, both in NF and FF.

	Pressure (bar)	d_{DLS} (nm)	PdI
NF	1.5	506.8 ± 13.9	0.6
	2.3	229.4 ± 8.6	0.4
	4.0	197.7 ± 44.9	0.4
FF	1.5	1444.3 ± 494.8	0.9
	2.3	809.3 ± 375.1	0.7
	4.0	375.5 ± 143.4	0.5

4. Conclusions

Here, a suspension based on nanoscale TiO_2 was applied by spray deposition under different experimental conditions, in order to produce nanostructured antibacterial textiles. During the spray process we assessed the influence of three main process parameters (pressure, web speed and number of working spray nozzles) on size distribution, concentration of particles released and LDSA of released particles. Further analysis of processed data obtained during monitoring measurements allowed comparing the collected data with the REL.

Particle number concentration and LDSA data showed the pressure at the spraying nozzles to be the main parameter that influences the

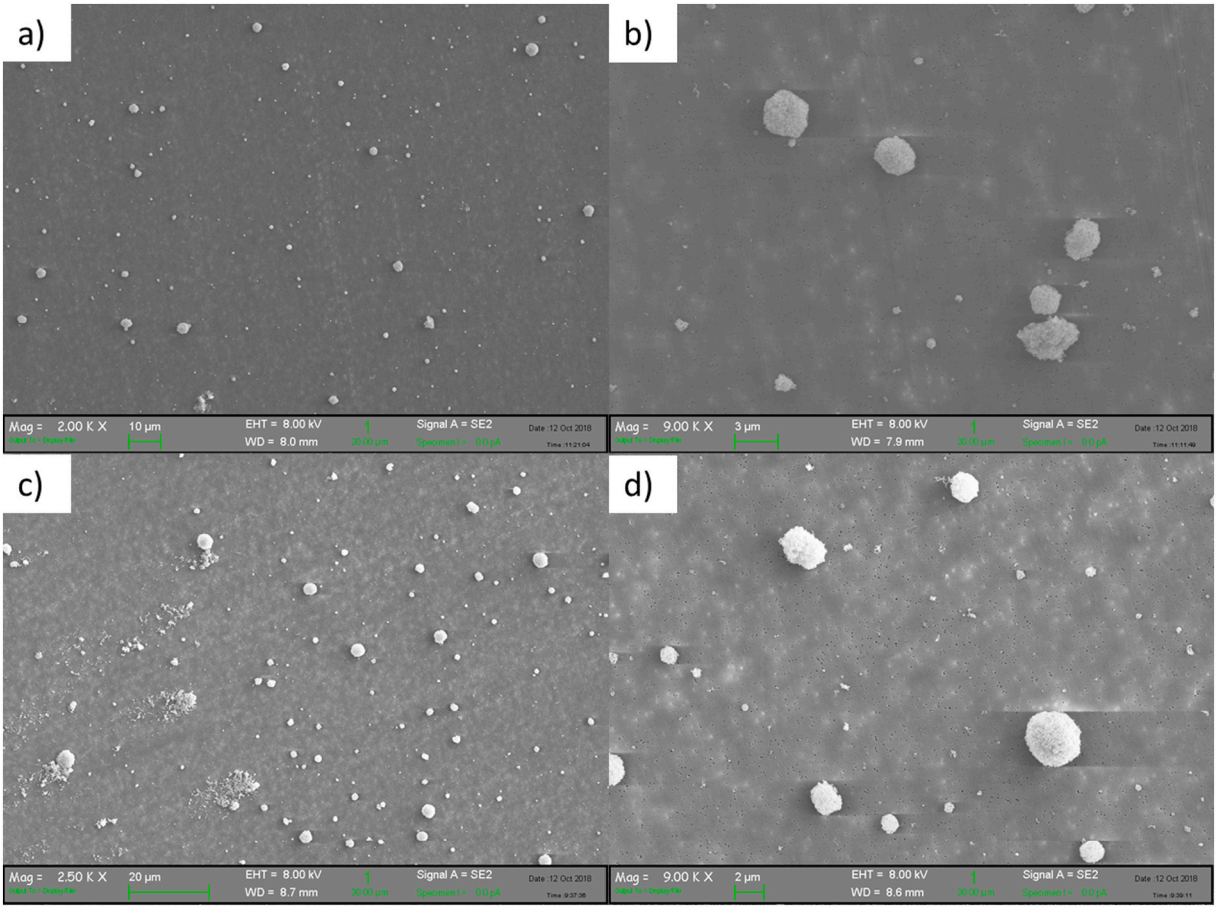

Fig. 6. FESEM images of different areas of filter, during five iterations at P = 1.5 bar. a)–b): FF; c)–d): NF.

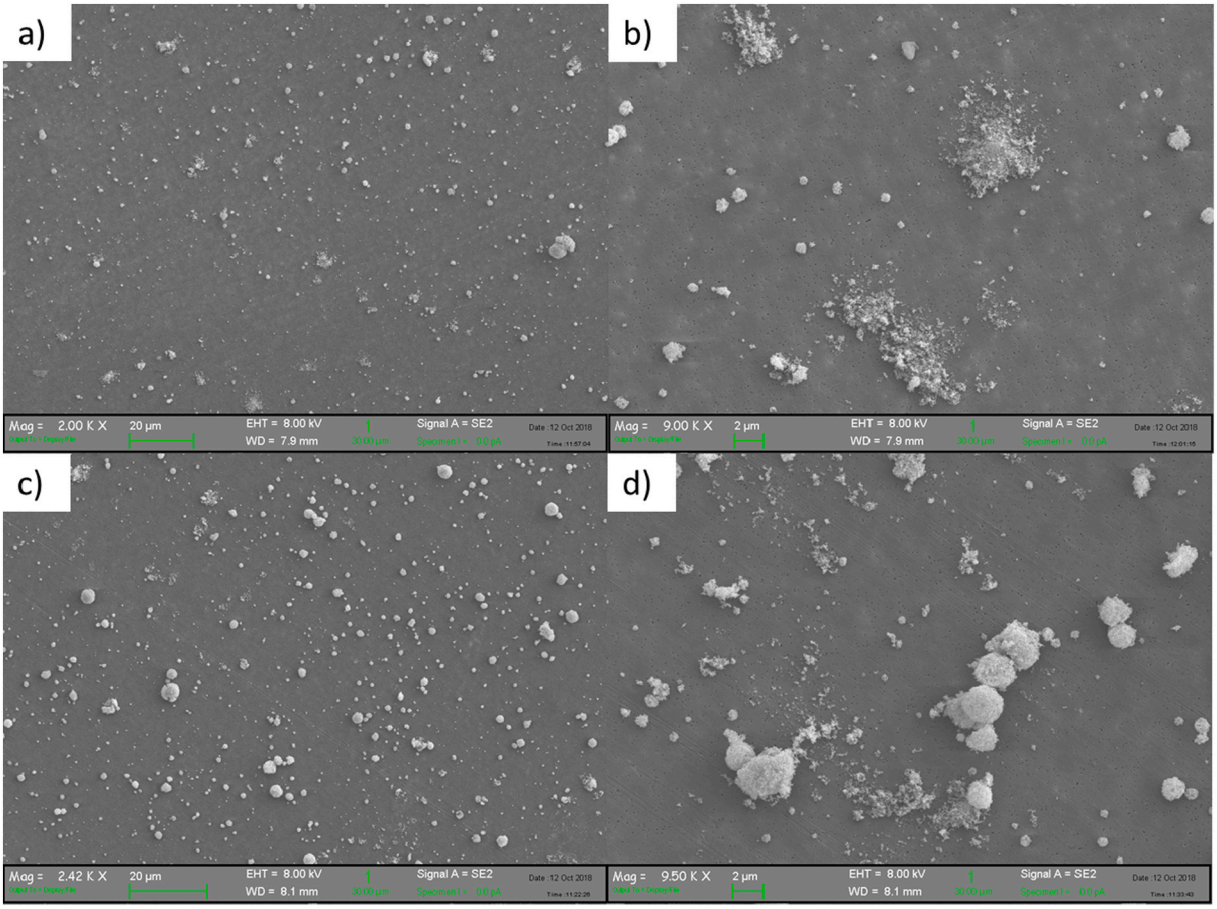

Fig. 7. FESEM images of different areas of filter, during five iterations at P = 2.3 bar. a)–b): FF; c)–d): NF.

release of particles in the environment. Upon increasing the pressure from 1.5 to 4.0 bar, average particle and LDSA concentrations varied from 4.3 10^5 to 1.2 10^6 particles/L and 51.8 to 290.5 $\mu m^2/cm^3$ in the near-field. Moreover, a decrease of particles size was found vs. increasing pressure, which trend was further confirmed by particle size distribution data obtained using DLS. Indeed, when increasing the pressure from 1.5 to 4.0 bar, the average diameter of particles from both NF and FF filters decreases (from 507 to198 nm and from 1.4 µm to 375 nm, respectively). Other process parameters studied (web speed and number of working spray nozzles) did not appear to significantly affect the release of particles. Nevertheless, we found an increase of particle size vs. increasing number of working spray nozzles likely due to coalescence phenomena induced by multi-nozzle spraying. OPC results translated into mass concentration confirmed that pressure was the main parameter affecting the release of particles during the spray deposition process. Considering the medium values of mass concentration as the biologically relevant TiO_2 dosimetry parameters, all values were found to be below the critical dose, even though the situation at the maximum value of pressure (P = 4.0 bar) looks critical, since during the spray coating process the maximum values are significantly out of range. Nevertheless, we should consider that workers are only present at the spray-coating plant for initial setting and occasional process checks. Thus it is reasonable to think that the workers are subjected to lower concentrations than those measured. However, in order to limit the emission of particles during the process, it is strongly recommended to confine the spray nozzles system inside a hood.

CRediT authorship contribution statement

Simona Ortelli: Methodology, Investigation, Data curation, Writing - original draft, Writing - review & editing.**Franco Belosi:**Methodology, Investigation, Data curation, Writing - review & editing, Supervision.**Rossella Bengalli:**Methodology, Investigation, Writing - review & editing.**Fabrizio Ravegnani:**Methodology, Investigation, Data curation, Writing - review & editing.**Carlo Baldisserri:**Methodology, Investigation, Data curation, Writing - review & editing.**Massimo Perucca:**Methodology, Investigation, Writing - review & editing, Funding acquisition.**Nuno Azoia:**Methodology, Investigation, Writing - review & editing.**Magda Blosi:**Writing - review & editing.**Paride Mantecca:**Conceptualization, Writing - review & editing, Supervision, Funding acquisition.**Anna Luisa Costa:**Conceptualization, Writing - review & editing, Supervision, Funding acquisition.

Declaration of competing interest

The authors declare that they have no known competing financial interests or personal relationships that could have appeared to influence the work reported in this paper.

Acknowledgement

This work was supported by the European Union's Horizon 2020 research and innovation programme through the project “PROTECT”, number 720851.

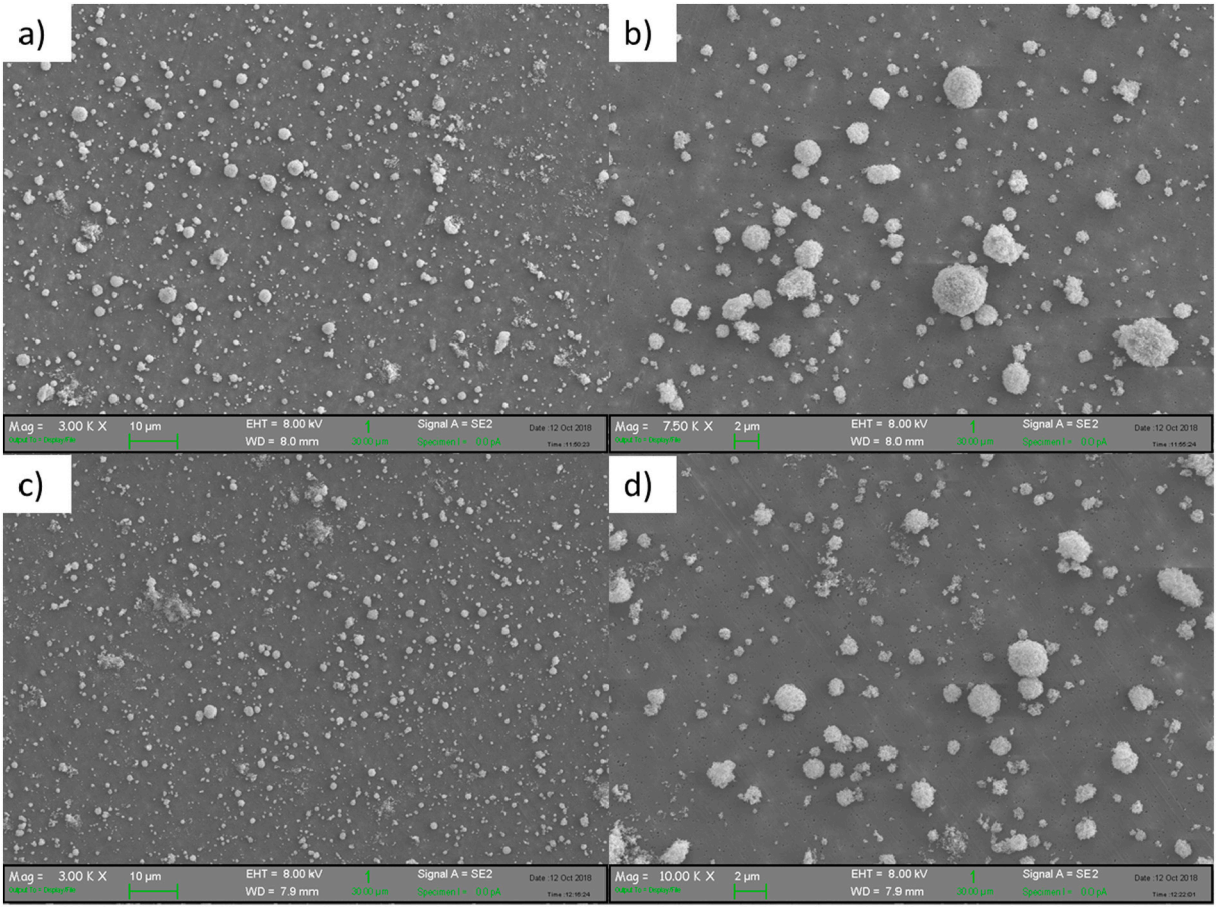

Fig. 8. FESEM images of different areas of filter, during five iterations at P = 4.0 bar. a)–b): FF; c)–d): NF.

Appendix A. Supplementary data

Supplementary data to this article can be found online at https://doi.org/10.1016/j.impact.2020.100245.

References

Asbach, C., Alexander, C., Clavaguera, S., Dahmann, D., Dozol, H., Faure, B., Fierz, M., Fontana, L., Iavicoli, I., Kaminski, H., MacCalman, L., Meyer-Plath, A., Simonow, B., van Tongeren, M., Todea, A.M., 2017. Review of measurement techniques and methods for assessing personal exposure to airborne nanomaterials in workplaces. Sci. Total Environ. 603–604, 793–806. https://doi.org/10.1016/j.scitotenv.2017.03.049.

Baranowska-Wójcik, E., Szwajgier, D., Oleszczuk, P., Winiarska-Mieczan, A., 2020. Effects of titanium dioxide nanoparticles exposure on human health—a review. Biol. Trace Elem. Res. 193, 118–129. https://doi.org/10.1007/s12011-019-01706-6.

Bekker, C., Brouwer, D.H., van Duuren-Stuurman, B., Tuinman, I.L., Tromp, P., Fransman, W., 2014. Airborne manufactured nano-objects released from commercially available spray products: temporal and spatial influences. J. Expo. Sci. Environ. Epidemiol. 24, 74–81. https://doi.org/10.1038/jes.2013.36.

Belut, E., Jiménez, A.S., Meyer-Plath, A., Koivisto, A.J., Koponen, I.K., Jensen, A.C.Ø., MacCalman, L., Tuinman, I., Fransman, W., Domat, M., Bivolarova, M., Tongeren, M. van, 2019. Indoor dispersion of airborne nano and fine particles: main factors affecting spatial and temporal distribution in the frame of exposure modeling. Indoor Air 29, 803–816. https://doi.org/10.1111/ina.12579.

Boccuni, F., Ferrante, R., Tombolini, F., Lega, D., Antonini, A., Alvino, A., Pingue, P., Beltram, F., Sorba, L., Piazza, V., Gemmi, M., Porcari, A., Iavicoli, S., 2018. Workers' exposure to nano-objects with different dimensionalities in R&D laboratories: measurement strategy and field studies. Int. J. Mol. Sci. 19, 349. https://doi.org/10.3390/ijms19020349.

Current intelligence bulletin 63: occupational exposure to titanium dioxide, 2011. NIOSH, National Institute for Occupational Safety and Health. Department of Health and Human Services. Public Health Service. Centers for Disease Control and Prevention. NIOSH Publication No. 2011–160https://doi.org/10.26616/NIOSHPUB2011160.

Donaldson, K., Stone, V., Clouter, A., Renwick, L., MacNee, W., 2001. Ultrafine particles. Occup. Environ. Med. 58, 211–216. https://doi.org/10.1136/oem.58.3.211.

Duffin, R., Tran, C.L., Clouter, A., Brown, D.M., MacNee, W., Stone, V., Donaldson, K., 2002. The importance of surface area and specific reactivity in the acute pulmonary inflammatory response to particles. Ann. Occup. Hyg 46, 242–245. https://doi.org/10.1093/annhyg/46.suppl_1.242.

EN 17058, 2018. Workplace Exposure - Assessment of Exposure by Inhalation of Nano-objects and Their Aggregates and Agglomerates ICS : [13.040.30].

Fissan, H., Neumann, S., Trampe, A., Pui, D.Y.H., Shin, W.G., 2007. Rationale and principle of an instrument measuring lung deposited nanoparticle surface area. J. Nanopart. Res. 9, 53–59. https://doi.org/10.1007/s11051-006-9156-8.

Fonseca, A.S., Viana, M., Querol, X., Moreno, N., de Francisco, I., Estepa, C., de la Fuente, G.F., 2015. Ultrafine and nanoparticle formation and emission mechanisms during laser processing of ceramic materials. J. Aerosol Sci. 88, 48–57. https://doi.org/10.1016/j.jaerosci.2015.05.013.

Foster, H.A., Ditta, I.B., Varghese, S., Steele, A., 2011. Photocatalytic disinfection using titanium dioxide: spectrum and mechanism of antimicrobial activity. Appl. Microbiol. Biotechnol. 90, 1847–1868. https://doi.org/10.1007/s00253-011-3213-7.

Francia, V., Martín, L., Bayly, A.E., Simmons, M.J.H., 2016a. Agglomeration in counter-current spray drying towers. Part a: particle growth and the effect of nozzle height. Powder Technol. 301, 1330–1343. https://doi.org/10.1016/j.powtec.2016.05.011.

Francia, V., Martín, L., Bayly, A.E., Simmons, M.J.H., 2016b. Agglomeration in counter-current spray drying towers. Part B: interaction between multiple spraying levels. Powder Technol. 301, 1344–1358. https://doi.org/10.1016/j.powtec.2016.05.010.

Francia, V., Martín, L., Bayly, A.E., Simmons, M.J.H., 2017. Agglomeration during spray drying: airborne clusters or breakage at the walls? Chem. Eng. Sci. 162, 284–299. https://doi.org/10.1016/j.ces.2016.12.033.

Geiss, O., Bianchi, I., Barrero-Moreno, J., 2016. Lung-deposited surface area concentration measurements in selected occupational and non-occupational environments. J. Aerosol Sci. 96, 24–37. https://doi.org/10.1016/j.jaerosci.2016.02.007.

Gwinn, M.R., Vallyathan, V., 2006. Nanoparticles: health effects—pros and cons. Environ. Health Perspect. 114, 1818–1825. https://doi.org/10.1289/ehp.8871.

Hagendorfer, H., Lorenz, C., Kaegi, R., Sinnet, B., Gehrig, R., Goetz, N.V., Scheringer, M., Ludwig, C., Ulrich, A., 2010. Size-fractionated characterization and quantification of nanoparticle release rates from a consumer spray product containing engineered nanoparticles. J. Nanopart. Res. 12, 2481–2494. https://doi.org/10.1007/s11051-009-9816-6.

Hama, S.M.L., Ma, N., Cordell, R.L., Kos, G.P.A., Wiedensohler, A., Monks, P.S., 2017. Lung deposited surface area in Leicester urban background site/UK: sources and contribution of new particle formation. Atmos. Environ. 151, 94–107. https://doi.org/10.1016/j.atmosenv.2016.12.002.

Hanot-Roy, M., Tubeuf, E., Guilbert, A., Bado-Nilles, A., Vigneron, P., Trouiller, B., Braun, A., Lacroix, G., 2016. Oxidative stress pathways involved in cytotoxicity and

genotoxicity of titanium dioxide (TiO2) nanoparticles on cells constitutive of alveolo-capillary barrier in vitro. Toxicol. Vitro Int. J. Publ. Assoc. BIBRA 33, 125–135. https://doi.org/10.1016/j.tiv.2016.01.013.

Hussein, T., Alameer, A., Jaghbeir, O., Albeitshaweesh, K., Malkawi, M., Boor, B.E., Koivisto, A.J., Löndahl, J., Alrifai, O., Al-Hunaiti, A., 2020. Indoor particle concentrations, size distributions, and exposures in middle eastern microenvironments. Atmosphere 11, 41. https://doi.org/10.3390/atmos11010041.

IARC Working Group on the Evaluation of Carcinogenic Risks to Humans, International Agency for Research on Cancer, World Health Organization, 2010. Carbon Black, Titanium Dioxide, and Talc, IARC Monographs on the Evaluation of Carcinogenic Risks to Humans. International Agency for Research on Cancer; Distributed by WHO Press, Lyon, France.

Ibald-Mulli, A., Wichmann, H.-E., Kreyling, W., Peters, A., 2002. Epidemiological evidence on health effects of ultrafine particles. J. Aerosol Med. 15, 189–201. https://doi.org/10.1089/089426802320282310.

Jensen, H., Pedersen, J.H., Jørgensen, J.E., Pedersen, J.S., Joensen, K.D., Iversen, S.B., Søgaard, E.G., 2006. Determination of size distributions in nanosized powders by TEM, XRD, and SAXS. J. Exp. Nanosci. 1, 355–373. https://doi.org/10.1080/17458080600752482.

Koivisto, A.J., Palomäki, J.E., Viitanen, A.-K., Siivola, K.M., Koponen, I.K., Yu, M., Kanerva, T.S., Norppa, H., Alenius, H.T., Hussein, T., Savolainen, K.M., Hämeri, K.J., 2014. Range-finding risk assessment of inhalation exposure to nanodiamonds in a laboratory environment. Int. J. Environ. Res. Public Health 11, 5382–5402. https://doi.org/10.3390/ijerph110505382.

Koivisto, A.J., Kling, K.I., Fonseca, A.S., Bluhme, A.B., Moreman, M., Yu, M., Costa, A.L., Giovanni, B., Ortelli, S., Fransman, W., Vogel, U., Jensen, K.A., 2018. Dip coating of air purifier ceramic honeycombs with photocatalytic TiO2 nanoparticles: a case study for occupational exposure. Sci. Total Environ. 630, 1283–1291. https://doi.org/10.1016/j.scitotenv.2018.02.316.

Koivisto, A.J., Kling, K.I., Hänninen, O., Jayjock, M., Löndahl, J., Wierzbicka, A., Fonseca, A.S., Uhrbrand, K., Boor, B.E., Jiménez, A.S., Hämeri, K., Maso, M.D., Arnold, S.F., Jensen, K.A., Viana, M., Morawska, L., Hussein, T., 2019. Source specific exposure and risk assessment for indoor aerosols. Sci. Total Environ. 668, 13–24. https://doi.org/10.1016/j.scitotenv.2019.02.398.

Kuhlbusch, T.A.J., Wijnhoven, S.W.P., Haase, A., 2018. Nanomaterial exposures for worker, consumer and the general public. NanoImpact 10, 11–25. https://doi.org/10.1016/j.impact.2017.11.003.

LeBlanc, A.J., Moseley, A.M., Chen, B.T., Frazer, D., Castranova, V., Nurkiewicz, T.R., 2010. Nanoparticle inhalation impairs coronary microvascular reactivity via a local reactive oxygen species-dependent mechanism. Cardiovasc. Toxicol. 10, 27–36. https://doi.org/10.1007/s12012-009-9060-4.

Losert, S., von Goetz, N., Bekker, C., Fransman, W., Wijnhoven, S.W.P., Delmaar, C., Hungerbuhler, K., Ulrich, A., 2014. Human exposure to conventional and nano-particle-containing sprays—a critical review. Environ. Sci. Technol. 48, 5366–5378. https://doi.org/10.1021/es5001819.

Nazarenko, Y., Lioy, P.J., Mainelis, G., 2014. Quantitative assessment of inhalation exposure and deposited dose of aerosol from nanotechnology-based consumer sprays. Environ. Sci. Nano 1, 161. https://doi.org/10.1039/c3en00053b.

Nijdam, J.J., Guo, B., Fletcher, D.F., Langrish, T.A.G., 2004. Challenges of simulating droplet coalescence within a spray. Dry. Technol. 22, 1463–1488. https://doi.org/10.1081/DRT-120038736.

Nuyttens, D., Baetens, K., De Schampheleire, M., Sonck, B., 2007. Effect of nozzle type, size and pressure on spray droplet characteristics. Biosyst. Eng. 97, 333–345. https://doi.org/10.1016/j.biosystemseng.2007.03.001.

Nymark, P., Bakker, M., Dekkers, S., Franken, R., Fransman, W., García-Bilbao, A., Greco, D., Gulumian, M., Hadrup, N., Halappanavar, S., Hongisto, V., Hougaard, K.S., Jensen, K.A., Kohonen, P., Koivisto, A.J., Maso, M.D., Oosterwijk, T., Poikkimäki, M., Rodriguez-Llopis, I., Stierum, R., Sørli, J.B., Grafström, R., 2020. Toward rigorous materials production: new approach methodologies have extensive potential to improve current safety assessment practices. Small 16, 1904749. https://doi.org/10.1002/smll.201904749.

Oberdörster, G., Sharp, Z., Atudorei, V., Elder, A., Gelein, R., Kreyling, W., Cox, C., 2004. Translocation of inhaled ultrafine particles to the brain. Inhal. Toxicol. 16, 437–445. https://doi.org/10.1080/08958370490439597.

Oberdürster, G., 2000. Toxicology of ultrafine particles: *in vivo* studies. Philos. Trans. R. Soc. Lond. Ser. Math. Phys. Eng. Sci. 358, 2719–2740. https://doi.org/10.1098/rsta.2000.0680.

OECD, 2015. Harmonized Tiered Approach to Measure and Assess the Potential Exposure to Airborne Emissions of Engineered Nano-objects and Their Agglomerates and Aggregates at Workplaces, Series on the Safety of Manufactured Nanomaterials No. 55.

Ortelli, S., Blosi, M., Delpivo, C., Gardini, D., Dondi, M., Gualandi, I., Tonelli, D., Aina, V., Fenoglio, I., Gandhi, A.A., Tofail, S.A.M., Costa, A.L., 2014. Multiple approach to test nano TiO2 photo-activity. J. Photochem. Photobiol. Chem. 292, 26–33. https://doi.org/10.1016/j.jphotochem.2014.07.006.

Park, J., Ham, S., Jang, M., Lee, J., Kim, Sunju, Kim, Sungkyoon, Lee, K., Park, D., Kwon, J., Kim, H., Kim, P., Choi, K., Yoon, C., 2017. Spatial–temporal dispersion of aerosolized nanoparticles during the use of consumer spray products and estimates of inhalation exposure. Environ. Sci. Technol. 51, 7624–7638. https://doi.org/10.1021/acs.est.7b00211.

Pope III, C.A., Dockery, D.W., 2006. Health effects of fine particulate air pollution: lines that connect. J. Air Waste Manag. Assoc. 56, 709–742. https://doi.org/10.1080/10473289.2006.10464485.

Santolaya, J.L., García, J.A., Calvo, E., Cerecedo, L.M., 2013. Effects of droplet collision phenomena on the development of pressure swirl sprays. Int. J. Multiph. Flow 56, 160–171. https://doi.org/10.1016/j.ijmultiphaseflow.2013.06.007.

Schmid, O., Stoeger, T., 2016. Surface area is the biologically most effective dose metric for acute nanoparticle toxicity in the lung. J. Aerosol Sci., Inhaled Particle Dosimetry 99, 133–143. https://doi.org/10.1016/j.jaerosci.2015.12.006.

Simeone, F.C., Blosi, M., Ortelli, S., Costa, A.L., 2019. Assessing occupational risk in designs of production processes of nano-materials. NanoImpact 14, 100149. https://doi.org/10.1016/j.impact.2019.100149.

Stoccoro, A., Di Bucchianico, S., Coppedè, F., Ponti, J., Uboldi, C., Blosi, M., Delpivo, C., Ortelli, S., Costa, A.L., Migliore, L., 2017. Multiple endpoints to evaluate pristine and remediated titanium dioxide nanoparticles genotoxicity in lung epithelial A549 cells. Toxicol. Lett. 276, 48–61. https://doi.org/10.1016/j.toxlet.2017.05.016.

Todea, A.M., Beckmann, S., Kaminski, H., Bard, D., Bau, S., Clavaguera, S., Dahmann, D., Dozol, H., Dziurowitz, N., Elihn, K., Fierz, M., Lidén, G., Meyer-Plath, A., Monz, C., Neumann, V., Pelzer, J., Simonow, B.K., Thali, P., Tuinman, I., van der Vleuten, A., Vroomen, H., Asbach, C., 2017. Inter-comparison of personal monitors for nanoparticles exposure at workplaces and in the environment. Sci. Total Environ. 605–606, 929–945. https://doi.org/10.1016/j.scitotenv.2017.06.041.

Ulrich, A., Losert, S., Bendixen, N., Al-Kattan, A., Hagendorfer, H., Nowack, B., Adlhart, C., Ebert, J., Lattuada, M., Hungerbühler, K., 2012. Critical aspects of sample handling for direct nanoparticle analysis and analytical challenges using asymmetric field flow fractionation in a multi-detector approach. J. Anal. At. Spectrom. 27, 1120. https://doi.org/10.1039/c2ja30024a.

Viana, M. (Ed.), 2016. Indoor and Outdoor Nanoparticles: Determinants of Release and Exposure Scenarios, the Handbook of Environmental Chemistry. Springer International Publishing. https://doi.org/10.1007/978-3-319-23919-4.

Visai, L., De Nardo, L., Punta, C., Melone, L., Cigada, A., Imbriani, M., Arciola, C.R., 2011. Titanium oxide antibacterial surfaces in biomedical devices. Int. J. Artif. Organs 34, 929–946. https://doi.org/10.5301/ijao.5000050.